Cellular Physiology and Biochemistry

Cell Physiol Biochem 2018;47:83-96
DOI: 10.1159/000489751
Published online: May 15, 2018
Accepted: March 16, 2018

Original Paper

5-Aminolevulinic Acid-Mediated Sonodynamic Therapy Alleviates Atherosclerosis via Enhancing Efferocytosis and Facilitating a Shift in the Th1/Th2 Balance Toward Th2 Polarization

Yang Yang[a] Yuanyuan Liu[a,d] Xi Chen[a] Jie Gong[b] Zhen Huang[a] Wei Wang[a] Yuanqi Shi[a] Yu Wang[a] Jianting Yao[a] Zhaoqian Shen[a] Zhen Tian[b] Hong Jin[e] Ye Tian[a,b,c]

[a]Department of Cardiology, The First Affiliated Hospital, Cardiovascular Institute, Harbin Medical University, [b]Department of Pathophysiology and the Key Laboratory of Cardiovascular Pathophysiology, Harbin Medical University, the Key Laboratory of Cardiovascular Research (Harbin Medical University), Ministry of Education, [c]Heilongjiang Academy of Medical Sciences, Harbin, [d]Department of Cardiology, Heilongjiang Provincial Hospital, Harbin, P. R. China, [e]Karolinska Institute, Department of Medicine, Stockholm, Sweden

Key Words
Sonodynamic therapy • Apoptosis • Reactive oxygen species • Atherosclerosis • T helper polarization

Abstract
Background/Aims: We and other groups have demonstrated that 5-aminolevulinic acid (ALA)-mediated sonodynamic therapy (ALA-SDT) induces macrophage and foam cell apoptosis and stabilizes atherosclerosis (AS) plaques in animal models. Lymphocytes also play vital roles in the development of AS. The primary purpose of the present study was to investigate the effects of ALA-SDT on T helper (Th) cell fate and function, Th subset differentiation, and atherosclerotic lesion stability. ***Methods:*** We utilized ALA-SDT on Western diet-fed apoE$^{-/-}$ mice *in vivo* and human Jurkat cells *in vitro*. Hematoxylin and eosin staining and TUNEL assays were used to evaluate the atherosclerotic plaque size and apoptosis within the atheroma. ALA induced cytotoxicity on cultured Jurkat cells was determined with CCK-8 assay. To address the mechanisms, levels of intracellular reactive oxygen species (ROS), mitochondrial membrane potential (MMP), and mitochondrial permeability transition pore (MPTP) opening were evaluated by staining with fluorescent probes. Western blot analysis and confocal microscopy were used to analyze the protein levels of caspases, Bax and cytochrome c and the release of cytochrome c. Cell apoptosis and necrosis and phagocytosis were examined by flow cytometry.

Y. Yang, Y. Liu and X. Chen contributed equally to this work.

Ye Tian
Dept. of Cardiology, The First Affiliated Hospital, Cardiovascular Institute, Harbin Med. Univ.
23 Youzheng Street, Harbin 150001 (China)
Tel.+86-451-85555943, Fax +86-451-87530341, E-Mail yetian@ems.hrbmu.edu.cn

ELISAs and immunofluorescent staining were used to assess the corresponding cytokine levels and Th subset cell numbers within the atheroma. ***Results:*** Our studies revealed that ALA-SDT significantly enhanced $CD4^+$ cell apoptosis and macrophage-mediated phagocytosis and hence reduced the necrotic core size. ALA-SDT activated the mitochondrial apoptotic signaling pathway with minimal necrosis in Jurkat cells. ALA-SDT inhibited the Th1 response and enhanced the Th2 response. These effects of ALA-SDT were mediated primarily through the generation of ROS. ***Conclusion:*** ALA-SDT alleviates AS by enhancing cytotoxic effects on Th cells, subsequently stimulating efferocytosis and facilitating a shift in the Th1/Th2 balance toward Th2 cells, a discovery that might help elucidate the mechanism underlying SDT as a potential treatment to prevent atherothrombotic events.

Introduction

Ischemic heart disease (IHD) and stroke due to vulnerable atherosclerotic plaque rupture are the two leading causes of morbidity and mortality worldwide. These conditions are estimated to be responsible for one-quarter of all deaths annually. In addition, the total number of deaths from IHD and stroke are increasing globally [1-3]. Atherosclerosis (AS) is defined as a slowly progressive chronic inflammatory disease occurring in the walls of large and medium-sized arteries that arises from an imbalance in lipid metabolism and a maladaptive inflammatory response [4, 5]. T lymphocytes, a cellular minority, especially $CD4^+$ T helper (Th) cells, are present in human plaques and are known to function decisively in the regulation of inflammation during atherogenesis [5, 6].

According to the signature cytokines produced, as well as their functions, activated Th cells are mainly defined by interferon (IFN)-γ secreted from Th1 cells and interleukin (IL)-4 from Th2 cells [7]. The Th1-cell response mediated by IFN-γ promotes macrophage activation and the production of pro-atherogenic inflammation mediators and counteracts cap formation by enhancing protease and chemokine secretion and collagen degradation. Attenuated atherosclerosis development appears in IFN-γ-deficient atherosclerosis-prone mice and in mice with genetic knockdown of the Th1-cell-associated transcription factor T-box expressed in T cells (T-bet) [8-11]. The Th2-cell-specific transcription factor GATA-binding protein 3 (Gata-3) plays a pivotal role in the differentiation of Th2, upregulates IL-4 and IL-5, and inhibits the production of IFN-γ. Cytokines released from Th2 cells, including IL-10, IL-13 and IL-25, suppress vascular inflammation and atherosclerosis. In addition, promotion of a Th2 cell response in hyperlipidemic mice inhibits atherosclerotic lesion development [12, 13]. Therefore, the equilibrium between these two subsets may influence the development of atherosclerotic plaques, and increasing regulation of Th1/Th2 may provide a novel therapeutic strategy for AS.

Low-intensity ultrasound combined with the chemical compound 'sonosensitizer,' termed sonodynamic therapy (SDT), has been widely used in cancer treatments [14-17]. Many studies have demonstrated that SDT has great potential as a non-invasive treatment due to the strong tissue-penetrating and regional focusing properties of ultrasound. Our group previously reported that 5-aminolevulinic acid (ALA)-mediated SDT (ALA-SDT) induces THP-1 macrophage and foam cell apoptosis via mitochondrial pathways [18, 19]. More importantly, we found that ALA-SDT could stabilize atherosclerotic plaques [20] and inhibit the progression of AS *in vivo* [21]. Although not as abundant as macrophages in human lesions, Th cells have been reported to play key roles in lesion growth and disease aggravation [22]. Information regarding the effects of ALA-SDT on immunologic function, especially on Th cell differentiation, is lacking. Therefore, the aim of this work was to determine whether ALA-SDT induces Th cell apoptosis and differentiation as well as Th cell-associated cytokine secretion in human lymphoblastoid Jurkat T cells and in $apoE^{-/-}$ mice.

Materials and Methods

Chemicals and antibodies:

5-Aminolevulinic acid (ALA), phytohemagglutinin (PHA), phorbol-12-myristate-13-acetate (PMA) and N-acetyl-L-cysteine (NAC) were obtained from Sigma-Aldrich (St Louis, MO, USA). Qualified fetal bovine serum (FBS) and RPMI 1640 medium were acquired from Gibco (Grand Island, NY, USA). (4R,6S, 8S,10Z,12R,14R,16E,18R,19R,20S,21S)-19, 21-Dihydroxy-22-{(2S,2′R,5S,5′S)-5′-[(1R)-1-hydroxyethyl]-2, 5′-dimethyloctahydro-2, 2′-bifuran-5-yl}-4, 6,8, 12, 14, 18, 20-heptamethyl-11-oxido-9-oxodocosa-10, 16-dienoic acid (Ionomycin) was purchased from Yeasen Biotechnology Co., Ltd. (Shanghai, China). An *in situ* cell death detection kit was acquired from Roche (Nutley, NJ, USA). We obtained a cell MPTP detection kit from GenMed Scientifics Inc. (Arlington, MA, USA), and a Cell Counting Kit-8 (CCK-8) was acquired from Dojindo Molecular Technologies, Inc. (Kumamoto, Japan). 5, 5',6, 6'-Tetrachloro-1, 1,3, 3'-tetraethylbenzimidazolyl-carbocyanine iodide (JC-1), Mito-Tracker Green, and 4, 6-diamidino-2-phenylindole (DAPI) were obtained from Beyotime Biotechnology (Beijing, China). Mito-Tracker Deep Red FM, Hoechst 33342, CellROX Green reagent and pHrodo™ Red SE were purchased from Molecular Probes (Carlsbad, CA, USA). A FITC Annexin V Apoptosis Detection Kit II was acquired from BD Biosciences Pharmingen (San Jose, CA, USA). Human IL-4 and IFN-γ ELISA kits were obtained from NeoBioscience Technology Co., Ltd. (Shenzhen, China). Antibodies against Gata-3 (D13C9), T-bet/TBX21 (D6N8B), caspase-3, caspase-9, cleaved caspase-3 and cleaved caspase-9 were acquired from Cell Signaling Technology (Beverly, MA, USA). Antibodies against CD4, IL-4 and IFN-γ were obtained from Abcam (Cambridge, UK). Antibodies against cytochrome c, HSP 60 and actin were purchased from Santa Cruz Biotechnology, Inc. (Santa Cruz, CA, USA). Super ECL reagent was obtained from HaiGene (Harbin, China). All secondary antibodies were acquired from Bioss Inc. (Beijing, China).

Mouse atherosclerosis model

Male C57BL/6J apoE$^{-/-}$ mice (6-8 weeks old) were obtained from Beijing Vital River Laboratory Animal Technology Co., Ltd., (Beijing, China) and housed in a specific pathogen-free environment. The mice were fed a Western-type diet (WD, 0.25% cholesterol, 19.5% casein, 21% fat, 34.16% sugar) for 12 weeks to develop advanced atherosclerotic plaques in the aortic root. The mice were randomly separated into one of two groups: the Control group or the SDT group (n=10 per group). SDT group mice were subjected to ultrasonic radiation for 15 min at 2 h following an injection of ALA (60 mg/kg) into the caudal vein. After SDT treatment, the mice were fed a normal diet. All animal experiments were performed in accordance with the regulations of the Harbin Medical University Human Ethics Committee. The use and care of the animals conformed to the US National Institutes of Health Guide for Care and Use of Laboratory Animals.

Cell culture and activation

The human Jurkat E6.1 T cell line was acquired from American Type Culture Collection (ATCC, Manassas, VA, USA). Jurkat E6.1 cells were cultured at a density of 2×10^6 cells/mL in RPMI 1640 medium containing 10% FBS, 20 units/mL penicillin and 20 μg/mL streptomycin and maintained at 37°C in a humidified atmosphere containing 5% CO_2. For activation, Jurkat cells were treated with 1 mg/mL PHA for 24 h, washed, and subsequently incubated in the presence of PMA (25 ng/mL) plus ionomycin (1 μg/mL) for another 24 h.

Sonication device and treatment protocol

Cells were exposed to ultrasound as described previously. Briefly, the ultrasonic generator, transducer and power amplifier used in this study were designed and assembled by the Harbin Institute of Technology (Harbin, China). The customized ultrasonic transducer (diameter: 3.5 cm; resonance frequency: 1.0 MHz; duty factor: 10%; repetition frequency: 100 Hz) was placed in a degassed water bath 30 cm away from the Petri dishes. The exposure time was 5 min.

Histopathology and terminal deoxynucleotidyl transferase dUTP Nick-End Labeling (TUNEL) assay

Vessel parameters of mice were evaluated through hematoxylin and eosin (H&E) staining. All slices were subjected to H&E staining according to routine histopathological methods.

Apoptotic cells in mouse aortic root sections were detected using an *in situ* cell death detection kit according to the manufacturer's instructions. Nuclei were counterstained with DAPI. For *in situ* efferocytosis

assays, cryosections were subjected to immunofluorescent staining of macrophages and TUNEL staining of apoptotic cells simultaneously. All lesions were observed under an Olympus microscope.

Cell viability assay

The cytotoxicity of ALA was determined by the CCK-8 assay according to the manufacturer's instructions. Concisely, Jurkat cells (2×10^5 cells/mL) were seeded into 96-well plates, and 0-10 mM ALA was added for 48 h in the dark. Then, 10 μL of CCK-8 solution was added into each well and incubated at 37°C for 1 h. The absorbance at 450 nm was measured using a microplate reader.

ALA uptake in Jurkat cells

To investigate the intracellular metabolic kinetics of ALA-PpIX, Jurkat cells were rinsed three times with phosphate-buffered saline (PBS) and incubated with 1.0 mM ALA in serum-free RPMI 1640 for different time intervals in the dark at 37°C. The cells were then rinsed and fixed with 4% paraformaldehyde for 30 min. The fluorescence of ALA-PpIX in Jurkat cells was observed using an Olympus microscope equipped with a filter with a 405-nm excitation wavelength and a 630-nm emission wavelength. The fluorescence intensity of ALA-PpIX in Jurkat cells was measured with a multimode microplate reader at an excitation wavelength of 405 nm and an emission wavelength of 630 nm. For determination of the subcellular localization of ALA-PpIX, Jurkat cells were co-stained with 200 nM Mito-tracker Green for 30 min and 1 μg/mL Hoechst 33342 for 20 min at 37°C in the dark after incubation with 1.0 mM ALA for 4 and 6 h. Subsequently, the Jurkat cells were visualized by laser scanning confocal microscopy (LSCM).

Apoptosis detection by flow cytometry

We stained cells using a FITC Annexin V Apoptosis Detection Kit II for the assessment of cell apoptosis and necrosis by flow cytometry according to the instructions of the supplier.

Seeded cells (6×10^5 cells/mL) were harvested, gently rinsed with cold PBS, re-suspended in 100 μL 1x binding buffer with 5 μL of Annexin V-FITC and 5 μL of propidium iodide (PI), and then incubated for 15 min in the dark at room temperature. Immediately afterward, the cells were analyzed with a FACSCalibur flow cytometer (BD Biosciences). Data analysis was performed using FlowJo software. For proper statistical analysis, more than 10, 000 cells per group were counted.

Reactive oxygen species (ROS) level determination

The production of intracellular ROS was determined using CellROX Green reagent. Briefly, cells were seeded in six-well plates at 2×10^5 cells/mL and incubated with CellROX Green reagent (5 μM) for 30 min after sonication. The cells were fixed in 4% formaldehyde solution for 20 min in the dark before detection. The fluorescence intensity of the CellROX Green reagent was measured using a multimode microplate reader with excitation and emission wavelengths of 485 and 520 nm, respectively. Fluorescence images were captured with a fluorescence microscope.

pHrodo SE apoptotic phagocytosis assay

For phagocytosis assays, Jurkat cells from each group were collected and labeled with 100 ng/mL pHrodo™ Red SE for 30 min with light protection, washed with PBS, resuspended in the supernatant from each group, and then added to bone marrow-derived macrophages (BMDM). After co-incubation with the Jurkat cells for 1 h, phagocytes were detached from Petri dishes, stained with Percp-anti-CD11b for 1 h on ice and then washed thoroughly with PBS. Cells were analyzed with a FACSCalibur flow cytometer immediately and assessed with FlowJo software.

Mitochondrial membrane potential (MMP, $\Delta\Psi_m$) assessment

The MMP was determined by staining with the JC-1 fluorescent probe according to the manufacturer's protocol. Jurkat cells were pre-treated with NAC for 1 h after ALA incubation and then exposed to ultrasound. Staining was performed using 10 mg/mL JC-1 for 20 min at 37°C in the dark immediately after ultrasonic treatment. The fluorescence intensity was measured by a multimode microplate reader at an excitation wavelength of 525 nm and an emission wavelength of 590 nm for red fluorescence and an excitation wavelength of 490 nm and an emission wavelength of 530 nm for green fluorescence. Images were then obtained using a fluorescence microscope.

Calcein/Co^{2+} assay for mitochondrial permeability transition pore (MPTP) opening

MPTP opening in Jurkat cells was detected using a calcein/Co^{2+} assay with a cell MPTP detection kit according to the manufacturer's instructions. Briefly, seeded cells (2×10^5 cells/mL) were rinsed three times with PBS, washed twice with reagent A from the kit, and then incubated with an intermixture of reagent B and C at 37°C for 20 min with light protection. The cells were then stained with DAPI for 20 min in the dark and washed twice with reagent A. Subsequently, the cells were visualized by LSCM.

Western blotting analysis

Whole-cell lysates and mitochondrial and cytosolic fractions were extracted as described previously [23]. The protein samples were mixed with 5x SDS loading buffer, separated via 8%, 10% or 12% SDS-PAGE gels, and electrotransferred to PVDF membranes at 300 mA. After blocking in 6% skim milk for 2 h, the membranes were incubated at 4°C overnight with primary antibodies against caspase-3 (1:1000), caspase-9 (1:1000), cleaved caspase-3 (1:1000), cleaved caspase-9 (1:1000), cytochrome c (1:400), T-bet (1:1000), Gata-3 (1:1000), actin (1:2000), and HSP 60 (1:500). Then, the membranes were rinsed and incubated with HRP-conjugated IgG secondary antibodies (1:3000) at room temperature for 1 h. The membranes were then rinsed and detection was performed using a BIO-RAD ChemiDoc™MP Imaging System (Universal Hood III, Bio-Rad Laboratories, Inc., Hercules, CA, USA) using Super ECL reagent. Actin was used as a loading control for the whole-cell lysates or cytosolic fraction, and HSP 60 was used for the mitochondrial fraction. Densitometric values were quantified using Image Lab software (version 6.0, Bio-Rad).

Immunofluorescence assay

For cytochrome c translocation analysis, after ALA-SDT treatment, seeded cells were stained with 100 nM Mito-Tracker Deep Red FM for 30 min, fixed with 4% paraformaldehyde for 30 min, and then blocked with 3% bovine serum albumin (BSA) for 30 min at room temperature. Then, the cells were washed and incubated with a rabbit polyclone primary antibody against cytochrome c (1:500) overnight at 4°C. Subsequently, the cells were washed thoroughly, incubated with a goat anti-rabbit IgG Alexa Fluor 488-conjugated secondary antibody for 1 h and then stained with DAPI for 20 min at 37°C in the dark. Finally, the samples were visualized by LSCM.

The frozen lesion sections of mouse aortic roots were subjected to immunofluorescence staining according to standard procedures. Briefly, cryosections were blocked with 10% goat/rabbit serum for 30 min at 37°C and then incubated overnight at 4°C with primary antibodies against CD4 (1:500), IFN-γ (1:500), IL-4 (1:400), T-bet (1:500), and Gata-3 (1:500), followed by co-incubation with FITC-conjugated and TRITC-conjugated secondary antibodies for 1 h and counterstaining with DAPI for 20 min at 37°C in the dark. Finally, the cryosections were visualized using fluorescence microscopy.

Enzyme-linked immunosorbent assay (ELISA)

For detection of the levels of cytokines, the cell supernatant was collected after treatment. The levels of IFN-γ and IL-4 were measured with ELISA kits according to the manufacturer's instructions.

Statistical analysis

All the experiments were repeated at least three times independently. The results are presented as the mean ± standard error of the mean (SEM) values. For the analysis of significant differences between two groups, Student's two-tailed t-test was applied. The differences among three or more groups were analyzed via one-way analysis of variance (ANOVA) followed by the Student–Newman–Keuls test when appropriate. Statistical evaluation was performed using Statistical Analysis System (SAS) software version 9.2 (SAS institute, Cary, NC). Statistical significance was determined by a P value <0.05.

Results

ALA-SDT reduces the necrotic core size and stimulates $CD4^+$ cells apoptosis and Th1-to-Th2 shifting in atherosclerotic plaques

We first investigated the effects of ALA-SDT on AS in WD-fed $apoE^{-/-}$ mice. H&E staining of aortic roots revealed significant reduction of the plaque and necrotic core area

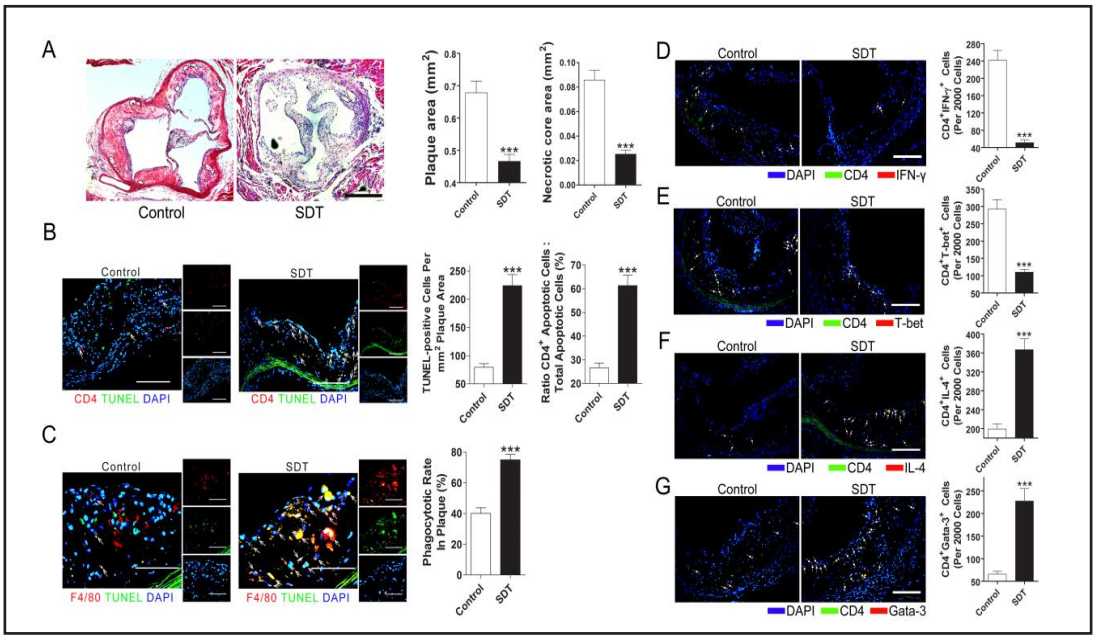

Fig. 1. ALA-SDT markedly inhibited the development of atherosclerosis in apoE$^{-/-}$ mice. (A) Atherosclerotic lesions in the different groups with H&E staining (left panel). Quantification of the plaque and necrotic core area is presented in the right penal. Scale bar: 500 μm. (B) Immunofluorescence (arrow, left panel) of plaque lesions double-stained for CD4 and TUNEL. Scale bar: 200 μm. Quantification (right panel) of TUNEL-positive apoptotic cells per mm^2 plaque area and the ratio of apoptotic CD4$^+$ cells to total apoptotic cells. (C) Immunofluorescence (arrow, left panel) and quantification (right panel) of macrophage-mediated phagocytosis of apoptotic cells. Scale bar: 100 μm. (D-G) Immunofluorescence (arrow, left panel) of plaque lesions double-stained for CD4 and IFN-γ, T-bet, IL-4 or Gata-3. Scale bar: 200 μm. Quantification of corresponding double-positive cells in murine plaques (right panel). The results are represented as the numbers of corresponding double-positive cells to the total cell number (per 2000 cells) within the atheroma. ***P<0.001 compared with the Control group.

in the SDT treated mice (P<0.001 vs. the Control group, Fig. 1A). We used a TUNEL assay to detect apoptotic cells in consecutive sections of the mouse aortic root. As shown in Fig. 1B, ALA-SDT significantly induced apoptosis in atherosclerotic plaques (P<0.001 vs. the Control group). Furthermore, the percentage of CD4$^+$ apoptotic cells among total apoptotic cells was significantly increased in the SDT group (61.3 ± 4.5% vs. 26.6 ± 2.0%, P<0.001). Efferocytosis of apoptotic cells prevents necrotic core formation and leads to the resolution of inflammation. Indeed, we observed significantly enhanced efferocytosis in SDT treated plaques (P<0.001 vs. the Control group, Fig. 1C). With further histological analysis, we observed that ALA-SDT reduced the number (per 2000 cells within the atheroma) of IFN-γ-producing CD4$^+$ cells (241.8 ± 22.5 vs. 51.3 ± 6.9, P<0.001, Fig. 1D) and CD4$^+$T-bet$^+$ cells (292.2 ± 27.1 vs. 100.2 ± 8.0, P<0.001, Fig. 1E). Furthermore, the numbers of IL-4-producing CD4$^+$ cells (199.0 ± 11.2 vs. 366.8 ± 23.3, P<0.001, Fig. 1F) and CD4$^+$Gata-3$^+$ cells (65.8 ± 6.3 vs. 227.5 ± 27.7, P<0.001, Fig. 1G) increased in the plaques of SDT treated mice compared with those of Control mice.

Optimization of SDT parameters

To investigate more cellular specific phenotype, we utilized ALA-SDT on human Jurkat cells *in vitro*. We first compared the effects of different ultrasonic intensities on cell viability using flow cytometry with Annexin V and PI double staining *in vitro*. As shown in Fig. 2A and B, there was no significant alteration in apoptotic ratio among different intensity cells. When the intensity of ultrasound was greater than 0.8 W/cm^2, the necrotic ratio gradually

rose as the amount of ultrasonic intensity increased (P<0.05, the 1.2 W/cm^2 group vs. the ultrasound untreated group). We subsequently investigated the cytotoxicity of ALA, the biological precursor of protoporphyrin IX (PpIX), on Jurkat cells via a CCK8 assay. As shown in Fig. 2C, the viability was reduced significantly from 88.6 ± 1.6% (2.0 mM, P<0.001 vs. the ALA untreated group) to 64.0 ± 1.5% (10 mM). Therefore, the application of 1 mM ALA with 0.8 W/cm^2 ultrasonic intensity represented the optimal treatment parameters.

Intracellular metabolic kinetics and subcellular localization of ALA-PpIX in Jurkat cells

The fluorescence intensity of 1 mM ALA-PpIX observed under a fluorescence microscope and detected by a multimode microplate reader increased over time and peaked at 6 h in Jurkat cells and then faded over time (Fig. 3A, B). We also observed the subcellular localization of ALA-PpIX in Jurkat cells. As shown in Fig. 3C, the red PpIX fluorescence partially overlapped with the green fluorescence emitted by the mitochondrial probe after incubation with ALA

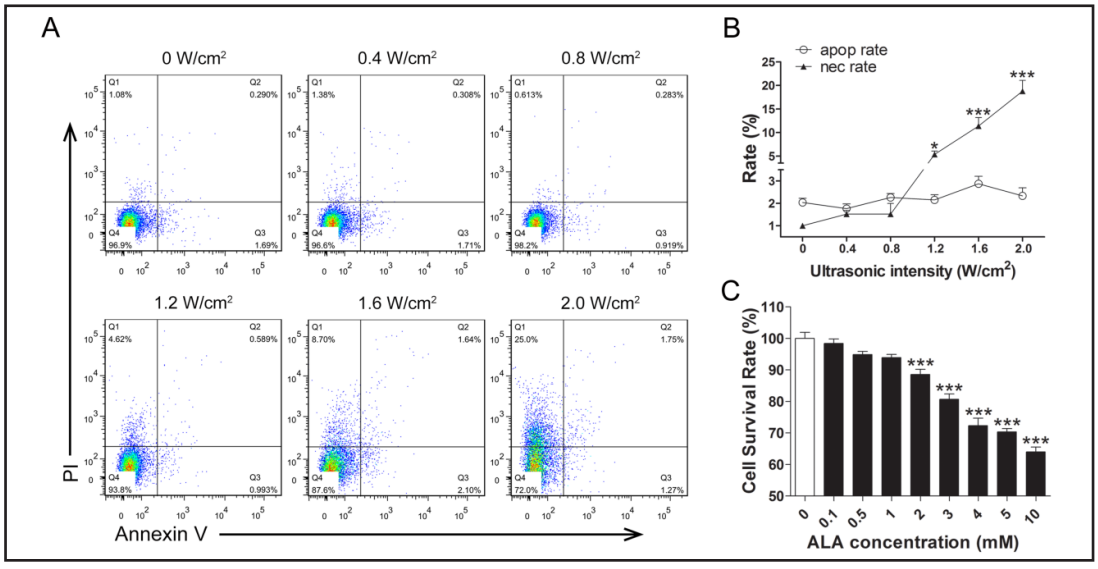

Fig. 2. Optimal ultrasound intensity and ALA concentration. (A) Representative flow cytograms of the effects of ultrasound alone on cell death of Jurkat cells. (B) Apoptotic and necrotic rates at 4 h after ultrasonic sonication were determined by flow cytometry. (C) Cytotoxicity of different concentrations of ALA on Jurkat cells as examined by a CCK-8 assay. *P<0.05, ***P<0.001 compared with the untreated group.

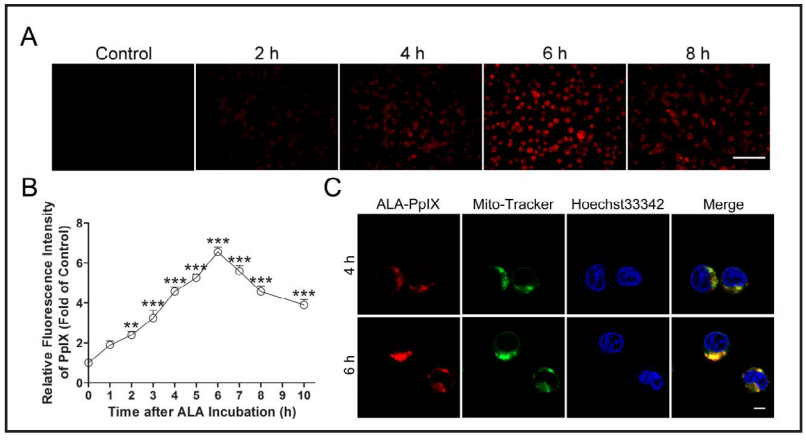

Fig. 3. Intracellular metabolic kinetics and subcellular localization of ALA-PpIX in Jurkat cells. (A) Representative photomicrographs of Jurkat cells showing intracellular ALA-PpIX after 1 mM ALA incubation for 2, 4, 6 and 8 h. Scale bar: 200 μm. (B) Quantitative measurements of the fluorescence intensity of ALA-PpIX in Jurkat cells for different time intervals after incubation with 1 mM ALA detected by a multimode microplate reader. (C) Representative fluorescent photomicrographs of the subcellular localization of ALA-PpIX in Jurkat cells visualized by LSCM. Scale bar: 5 μm. **P<0.01, ***P<0.001 compared with the untreated group.

for 4 h and was almost exclusively distributed in the mitochondria after 6 h of incubation when intracellular ALA-PpIX fluorescence intensity reached the maximum.

ALA-SDT induces intracellular ROS production

To investigate whether ALA-SDT elevates the level of ROS in Jurkat cells, the fluorescence intensity of CellROX was measured via fluorescence microscopy and a multimode microplate reader. As shown in Fig. 4B, relative ROS levels did not dramatically increase in either the ALA alone group (118.8 ± 2.6%) or ultrasound alone group (137.3 ± 4.1%) compared with the Control group (100 ± 2.6%), but increased significantly in the SDT group (461.1 ± 17.2%, $P<0.001$ vs. the Control). The results of fluorescence microscopy were consistent with those of the multimode microplate reader (Fig. 4A).

ALA-SDT induces late apoptosis of Jurkat cells and stimulates phagocytosis by macrophages

Cell apoptosis and necrosis were determined by flow cytometry with double staining of Annexin V and PI. Cells in the lower-right quadrant (Annexin V^+/PI^-) represent early

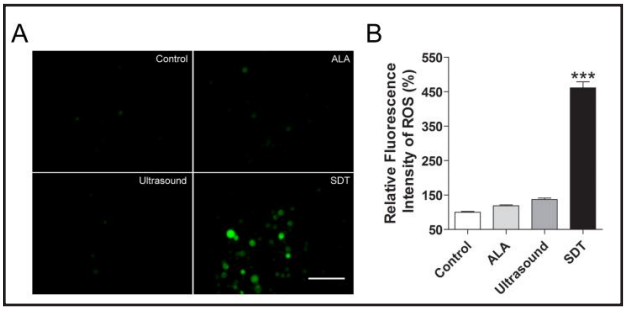

Fig. 4. Intracellular ROS production induced by ALA-SDT. (A) Representative fluorescent photomicrographs of effects on ROS generation using fluorescent probe CellROX Green. Scale bar: 200 μm. (B) Quantitative measurements of CellROX fluorescence intensity by multimode microplate reader. ***P<0.001 compared with the Control group.

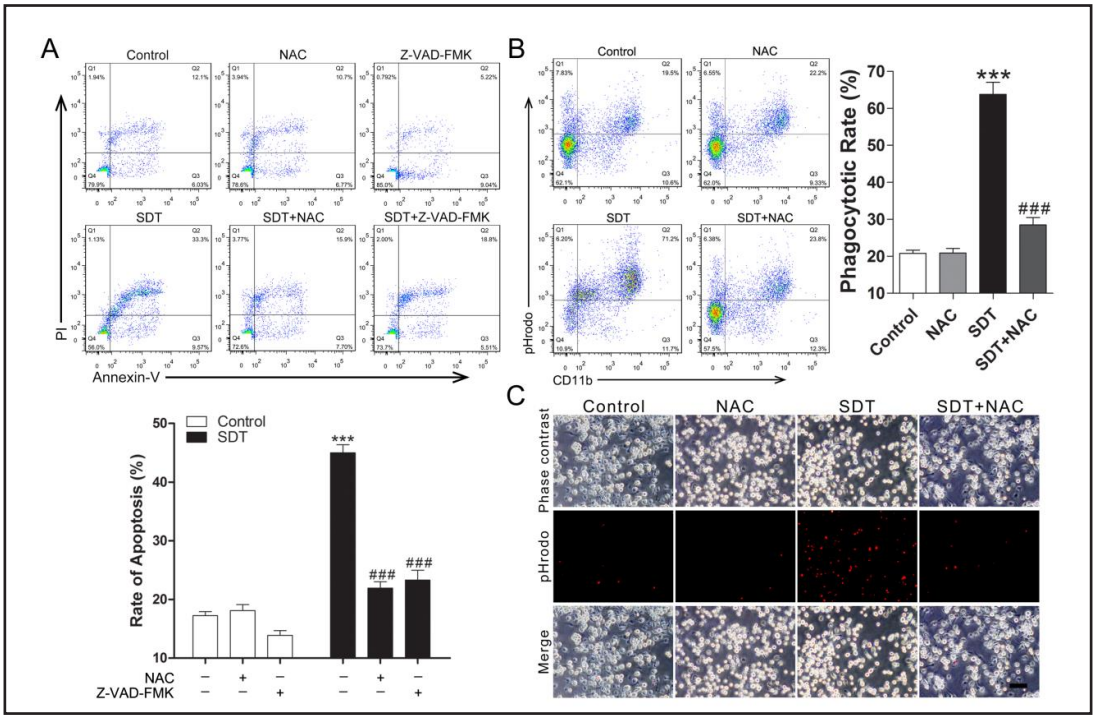

Fig. 5. Apoptosis induced by ALA-SDT. (A) Representative flow cytograms (upper panel) and quantification (lower panel) revealing cell death. (B) Representative flow cytograms (left panel) and quantification (right panel) revealing phagocytosis of Jurkat T cells in different groups induced by BMDM. (C) Phagocytosis of Jurkat T cells in different groups induced by BMDM. Scale bar: 80 μm. ***P<0.001 compared with the Control group. ###P<0.001 compared with the SDT group.

apoptotic cells, and those in the upper-right quadrant (Annexin V^+/PI^+) represent late apoptotic cells. As shown in Fig. 5A, the apoptotic ratio, particularly the late apoptotic ratio, of the SDT treated cells (45 ± 1.4%) was considerably higher compared to that of Control cells (17.2 ± 0.7%, P<0.001). Moreover, pretreatment with the ROS scavenger NAC attenuated apoptosis induced by ALA-SDT (21.9 ± 1.1%, P<0.001 vs. the SDT) effectively. Similarly, enhanced apoptosis was greatly suppressed by pretreatment with the pan-caspase inhibitor Z-VAD-FMK (23.3 ± 1.7%, P<0.001 vs. the SDT group) as well. The necrotic ratio did not significantly change among the experimental groups. We subsequently examined the phagocytosis of Jurkat T cells in different groups by BMDM and found that apoptotic cell uptakes increased to 63.8 ± 3.2% in the SDT group (P<0.001 vs. the Control group, Fig. 5B and C). NAC pretreatment (28.5 ± 2.0%, *P*<0.001 vs. the SDT group) significantly prevented SDT-induced phagocytosis.

ALA-SDT induces MMP collapse and mitochondrial permeability transition pore (MPTP) opening

As shown in Fig. 6A, most cells exhibited green fluorescence after SDT treatment, representing dissipation of the $\Delta\Psi_m$, whereas cells in the SDT plus NAC group displayed orange-red fluorescence due to a reversion of the $\Delta\Psi_m$ to normal levels. Consistent with this pattern, the results obtained using the multimode microplate reader showed that when cells were exposed to ALA-SDT, ΔΨm dissipated rapidly, and the ratio of red/green fluorescence intensity of JC-1 was notably increased in the SDT plus NAC group (11.2 ± 1.1) compared to the SDT group (5.5 ± 0.6, P<0.001, Fig. 6B). We next examined whether SDT could open the MPTP using the calcein/cobalt approach via LSCM. As shown in Fig. 6C, the calcein-dependent green fluorescence was markedly quenched by Co^{2+} in the SDT group. NAC pretreatment significantly prevented SDT-induced MPTP opening, as indicated by a remarkable reversion of dull calcein fluorescence to a bright signal.

ALA-SDT induces Bax translocation, cytochrome c release and caspase-3 and caspase-9 activation

Translocation of pro-apoptotic factor Bax from cytoplasm to mitochondria acts as a trigger of outer mitochondrial membrane permeabilization. Therefore, we analyzed

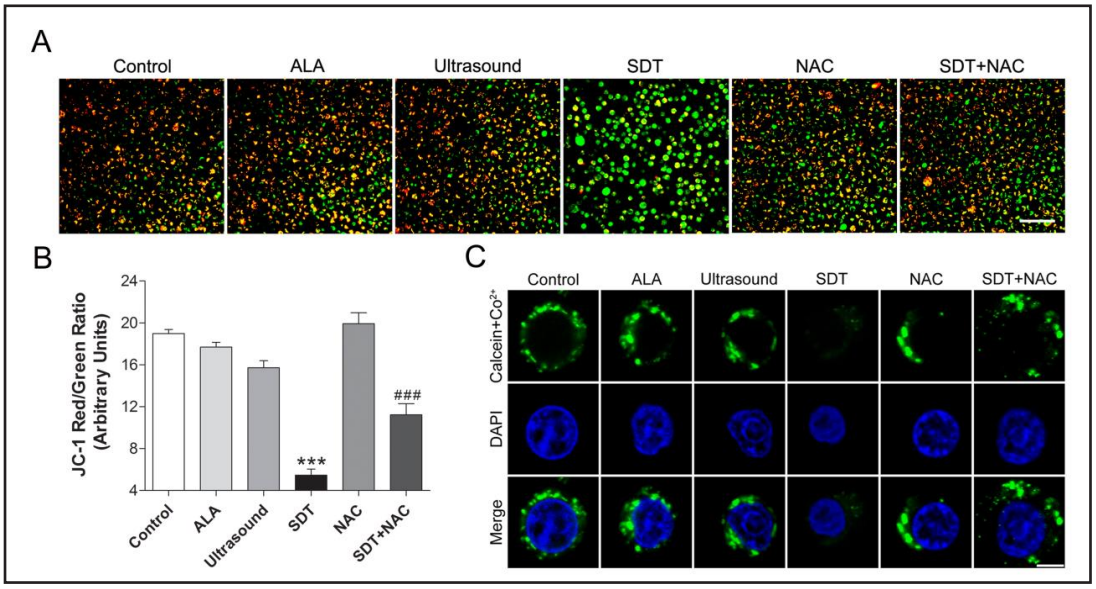

Fig. 6. Effects of ALA-SDT on mitochondrial membrane permeability. (A) Representative fluorescent photomicrographs of Jurkat cells stained with JC-1 showing MMP. Scale bar: 200 μm. (B) Quantitative measurements of MMP levels of Jurkat cells assessed with a multimode microplate reader. (C) Representative fluorescent photomicrographs of MPTP opening induced by ALA-SDT. Scale bar: 5 μm. ***P<0.001 compared with the Control group. ###P<0.001 compared with the SDT group.

the expression of Bax and cytochrome c in cytoplasm and mitochondria of Jurkat cells by Western blotting. A significant induction in mitochondria-localized Bax and a corresponding reduction in cytosolic Bax were observed in cells upon SDT, whereas the opposite pattern for cytochrome c was observed (Fig. 7A). NAC pretreatment, as expected, inhibited this SDT-induced Bax translocation to mitochondria as well as cytochrome c release into cytosol. Similar anti-apoptotic effects were observed for pretreatment with the singlet oxygen scavenger NaN_3. Cytochrome c release from mitochondria into cytosol was further supported by immunofluorescence staining; cells upon SDT modulation showed diffuse green fluorescence after ALA-SDT treatment (Fig. 7B), and this fluorescence was inhibited by pre-incubation with NAC and NaN_3. Moreover, we assessed the activation of caspase-3 and caspase-9 by Western blotting. ALA-SDT treatment notably induced the activation of both caspases. Pre-treatment with NAC or Z-VAD-FMK inhibited caspase-3 and caspase-9 activation induced by ALA-SDT (Fig. 7C).

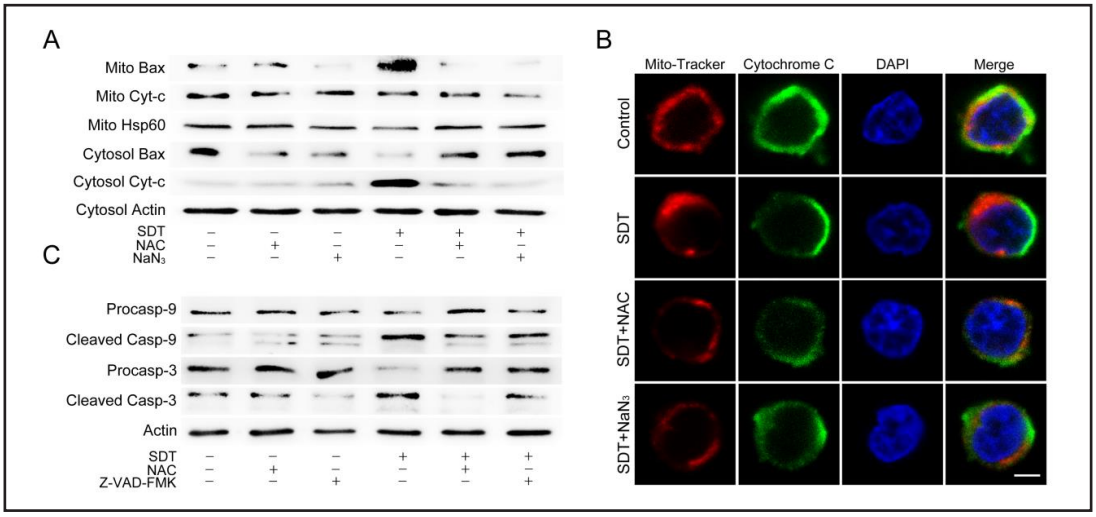

Fig. 7. Activation of the mitochondrial-caspase apoptosis pathway induced by ALA-SDT. (A) Protein levels of Bax and cytochrome c in mitochondrial and cytosolic fractions detected by Western blot analysis. (B) Representative LSCM images of cytochrome c release from mitochondria induced by ALA-SDT in Jurkat cells. Scale bar: 5 μm. (C) Representative Western blots of caspase-9, cleaved caspase-9, caspase-3 and cleaved caspase-3 protein expression.

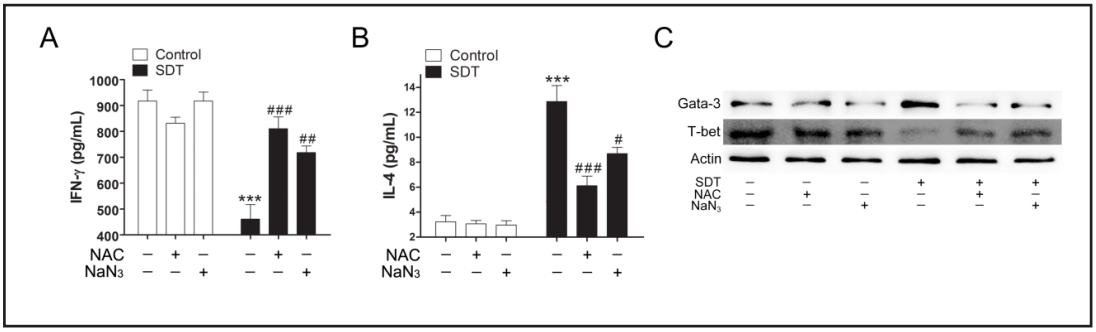

Fig. 8. A shift in the Th1/Th2 balance toward Th2 induced by ALA-SDT. (A) Quantitative measurements of the IFN-γ level in the supernatant of Jurkat cells in different treatment groups by ELISA. (B) Quantitative measurements of the IL-4 level in the supernatant of Jurkat cells in different treatment groups by ELISA. (C) Representative Western blots of T-bet and Gata-3 protein expression. ***P<0.001 compared with the Control group. #P<0.05, ##P<0.01, ###P<0.001 compared with the SDT group.

ALA-SDT facilitates a shift in the Th1/Th2 balance towards Th2 in vitro

As shown in Fig. 8A and B, the level of IFN-γ in supernatants of PMA plus ionomycin-activated Jurkat cells exposed to ALA-SDT (461.2 ± 55.9 pg/mL) was lower than that of control cells (917 ± 42.7 pg/mL, $P<0.001$ vs. the SDT group), but the cells treated with ALA-SDT (12.9 ± 1.3 pg/mL) secreted a higher level of IL-4 than the Control group (3.3 ± 0.5 pg/mL, $P<0.001$ vs. the SDT group). To further explore the mechanism of ALA-SDT-regulated Th cell polarization, changes in the expression of T-bet as well as Gata-3 are shown in Fig. 8C. ALA-SDT downregulated T-bet expression but upregulated Gata-3 expression *in vitro*. All of these effects were blocked by NAC or NaN_3 (Fig. 8A-C).

Discussion

Intriguing results from the Canakinumab Anti-Inflammatory Thrombosis Outcomes Study (CANTOS) recently showed that the IL-1 beta monoclonal antibody Canakinumab significantly reduced the incidence of adverse cardiovascular events in patients with myocardial infarction compared with the incidence in those treated with placebo, providing clinical trial evidence and indicating the significance of inflammation in AS pathology [24, 25]. Further investigation to identify novel efficient regimens that lessen inflammation in AS, therefore, is of great importance. We demonstrated in the present study that ALA-SDT efficiently regresses atherosclerotic plaque and improves the inflammatory environment within the atheroma by enhancing cytotoxic effects on Th cells, subsequently stimulating efferocytosis and facilitating a shift in the Th1/Th2 balance toward Th2 cells.

Our previous studies demonstrated that ALA-SDT induces apoptosis of macrophages and foam cells and stabilizes AS plaques in animal models [18-20]. In addition to macrophages, lymphocytes , primarily CD4-positive T cells are also vital participants throughout the course of atherosclerosis development [4]. In this study, we found that ALA could be metabolized into PpIX and accumulated in the mitochondria of Jurkat cells by 6 h after administration of 1 mM ALA (Fig. 3). The pattern of subcellular localization and the total level and peak time of PpIX accumulation in these cells was the same as that in the THP-1-derived foam cells [19], suggesting that ALA-SDT may simultaneously modulate both major types of cell function in atherosclerotic plaques and providing further evidence to utilize ALA-SDT in the lesion area on multi-dimensional targets.

In addition to synthesis rate, the specific subcellular localization patterns and tissue characteristics of the photosensitizer are important determinants of the efficacy of sonodynamic therapy [26-28]. We previously reported that ALA-derived PpIX mainly accumulates in the mitochondria of THP-1 macrophages and foam cells to induce mitochondrial damage [18, 19]. In the present study, we found that PpIX derived from the exogenous administration of ALA consistently aggregated in the mitochondria and activated the mitochondrial pathway of apoptosis in Jurkat cells. SDT-induced cellular damage seems to mainly depend on the specific subcellular localization patterns of the sonosensitizers. Activation of the sonosensitizer enhanced ROS formation in the binding site, determining the initially damaged subcellular organelles.

Expansion of the necrotic core contributes to the formation of vulnerable plaques and plaque disruption. Adequate phagocytosis of apoptotic cells by macrophages prevents necrotic core expansion and curbs atherosclerosis progression. However, if apoptotic cells are not efficiently removed by efferocytosis, these cells may undergo secondary necrosis, leading to larger necrotic cores and inflammation [29, 30]. In this study, ALA-SDT not only induced $CD4^+$ cell apoptosis but also stimulated macrophage-mediated phagocytosis of these apoptotic cells concurrent with the regression of lesion size and necrotic core size (Fig. 1A, B and C and Fig. 5). ALA-SDT directly or indirectly resolves inflammation via multiple mechanisms. First, ALA-SDT induces Th cell elimination, resulting in a decrease in inflammatory mediators, including IFN-γ. Second, enhanced efferocytosis inhibits post-apoptotic necrosis and prevents dead cells from releasing inflammatory contents. Third, the recognition of apoptotic cells activates anti-inflammatory mediators and anti-inflammatory

eicosanoids. Finally, ALA-SDT enhances the Th2 response, thereby suppressing vascular inflammation.

Accumulating evidence indicates that oxidative stress acts as an obligate second messenger, and the oxidative status of Th cells controls their effector functions, including cytokine production and subset differentiation [31-34]. Investigations both *in vivo* and *in vitro* have shown that ROS can preferentially promote Th2 skewing [35-37]. Moreover, natural antioxidant vitamin E suppresses Th2 responses upon T cell activation [38]. These studies highlight that ROS is an essential determinant of T helper differentiation and can dictate T helper bias. In the current study, ALA-SDT was shown to facilitate a shift in the Th1/Th2 balance toward Th2 *in vivo* and *in vitro* (Fig. 1D-G and Fig. 8). Here, we report for the first time the direct effects of ALA-SDT on naïve T cell differentiation. Moreover, our results demonstrated that ALA-SDT stimulated Th2-predominant responses, including modulation of the associated transcription factors that may be dependent on the production of ROS, particularly singlet oxygen (Fig. 8). Notably, recent studies have shown that ROS also function as intercellular messengers, and the extracellular oxidative microenvironment can influence cytokine generation in T cells. Activated macrophages can act as antigen-presenting cells for T cell priming, and the diffusion of ROS, such as H_2O_2, from macrophages to the T cells is necessary for this process during their close contact phase [31]. Thus, ROS derived from ALA-SDT in macrophages may be involved in the activation and polarization of Th cells. Further investigation regarding the intercellular signaling is undergoing in our laboratory.

Excessive levels of ROS lead to detrimental reactions with proteins, nucleic acids and lipids, playing an indispensable role in various cellular processes, including cell life and death decisions [39]. It is now clear that when exposed to ultrasound, the porphyrin-based sensitizers generate ROS, causing cytotoxicity [40]. Consistent with this finding, we found that ALA-SDT increased the intracellular ROS levels in Jurkat cells (Fig. 4). In addition, pre-incubation with NAC, an ROS scavenger, reversed ALA-SDT-mediated mitochondrial apoptotic signaling and T cell differentiation (Fig. 5-8). The ultrasound field is heterogeneous and ultrasonic waves can be reflected, and attenuated through a medium [41] and human tissue towards an atherosclerotic plaque. Cells at different distances or depths are exposed to different ultrasound fields. The different energies of SDT produce different ROS levels, thereby causing two distinct effects simultaneously, namely, pro-apoptotic effects and stimulation of Th1/Th2 shifting. We found that ALA-SDT induced Th cell apoptosis and enhanced macrophage-mediated phagocytosis of those apoptotic cells (Fig. 1A and B). Because Th1 predominates in advanced atherosclerotic plaques [42], ALA-SDT induced mostly Th1 cells apoptosis, but stimulated Th2-predominant responses, which could subsequently inhibit the Th1 response. Taken together, the results show that ALA-SDT plays a dual and synergistic role in modulating the Th1/Th2 equilibrium. In future, we plan to conduct more *in vivo* and *in vitro* experiments to distinguish the thresholds and spectra associated with distinct ROS level as well as their equivalent biological effects.

In summary, our results confirm that the optimization of ALA-SDT exerts cytotoxic effects on Th cells by selectively activating the mitochondrial apoptotic signaling pathway and enhancing macrophage-mediated phagocytosis. By inhibiting a Th1 response and favoring a Th2 response, ALA-SDT activated anti-inflammatory reactions, mainly through the generation of ROS. Our studies provide new insights into the mechanisms of SDT treatment as a novel therapeutic strategy for combating atherosclerosis.

Acknowledgments

This study was supported by the Major Research Equipment Development Project of National Natural Science of China (81727809), the State Key Project of National Natural Science of China (81530052), the National Natural Science Foundation of China (81371709) and the Major State Basic Research Development Program of China (2017YFB0403800). This study was also supported by the Graduate Student Innovative Research Project of Harbin Medical University (YJSCX2015-68HYD).

Disclosure Statement

The authors declare that they have no conflicts of interest to disclose.

References

1 Moran AE, Forouzanfar MH, Roth GA, Mensah GA, Ezzati M, Flaxman A, Murray CJ, Naghavi M: The global burden of ischemic heart disease in 1990 and 2010: The global burden of disease 2010 study. Circulation 2014;129:1493-1501.
2 Roth GA, Forouzanfar MH, Moran AE, Barber R, Nguyen G, Feigin VL, Naghavi M, Mensah GA, Murray CJ: Demographic and epidemiologic drivers of global cardiovascular mortality. N Engl J Med 2015;372:1333-1341.
3 Benjamin EJ, Blaha MJ, Chiuve SE, Cushman M, Das SR, Deo R, de Ferranti SD, Floyd J, Fornage M, Gillespie C, Isasi CR, Jimenez MC, Jordan LC, Judd SE, Lackland D, Lichtman JH, Lisabeth L, Liu S, Longenecker CT, Mackey RH, Matsushita K, Mozaffarian D, Mussolino ME, Nasir K, Neumar RW, Palaniappan L, Pandey DK, Thiagarajan RR, Reeves MJ, Ritchey M, Rodriguez CJ, Roth GA, Rosamond WD, Sasson C, Towfighi A, Tsao CW, Turner MB, Virani SS, Voeks JH, Willey JZ, Wilkins JT, Wu JH, Alger HM, Wong SS, Muntner P: Heart disease and stroke statistics-2017 update: A report from the american heart association. Circulation 2017;135:e146-e603.
4 Galkina E, Ley K: Immune and inflammatory mechanisms of atherosclerosis (*). Annu Rev Immunol 2009;27:165-197.
5 Hansson GK, Hermansson A: The immune system in atherosclerosis. Nat Immunol 2011;12:204-212.
6 Weber C, Zernecke A, Libby P: The multifaceted contributions of leukocyte subsets to atherosclerosis: Lessons from mouse models. Nat Rev Immunol 2008;8:802-815.
7 Daugherty A, Rateri DL: T lymphocytes in atherosclerosis: The yin-yang of th1 and th2 influence on lesion formation. Circ Res 2002;90:1039-1040.
8 Gupta S, Pablo AM, Jiang X, Wang N, Tall AR, Schindler C: Ifn-gamma potentiates atherosclerosis in apoe knock-out mice. J Clin Invest 1997;99:2752-2761.
9 Whitman SC, Ravisankar P, Daugherty A: Ifn-gamma deficiency exerts gender-specific effects on atherogenesis in apolipoprotein e-/- mice. J Interferon Cytokine Res 2002;22:661-670.
10 Buono C, Come CE, Stavrakis G, Maguire GF, Connelly PW, Lichtman AH: Influence of interferon-gamma on the extent and phenotype of diet-induced atherosclerosis in the ldlr-deficient mouse. Arterioscler Thromb Vasc Biol 2003;23:454-460.
11 Buono C, Binder CJ, Stavrakis G, Witztum JL, Glimcher LH, Lichtman AH: T-bet deficiency reduces atherosclerosis and alters plaque antigen-specific immune responses. Proc Natl Acad Sci U S A 2005;102:1596-1601.
12 Huber SA, Sakkinen P, David C, Newell MK, Tracy RP: T helper-cell phenotype regulates atherosclerosis in mice under conditions of mild hypercholesterolemia. Circulation 2001;103:2610-2616.
13 Schulte S, Sukhova GK, Libby P: Genetically programmed biases in th1 and th2 immune responses modulate atherogenesis. Am J Pathol 2008;172:1500-1508.
14 Yumita N, Nishigaki R, Umemura K, Umemura S: Hematoporphyrin as a sensitizer of cell-damaging effect of ultrasound. Jpn J Cancer Res 1989;80:219-222.
15 Lv Y, Fang M, Zheng J, Yang B, Li H, Xiuzigao Z, Song W, Chen Y, Cao W: Low-intensity ultrasound combined with 5-aminolevulinic acid administration in the treatment of human tongue squamous carcinoma. Cell Physiol Biochem 2012;30:321-333.
16 Courthion H, Mugnier T, Rousseaux C, Moller M, Gurny R, Gabriel D: Self-assembling polymeric nanocarriers to target inflammatory lesions in ulcerative colitis. J Control Release 2017
17 Wang X, Jia Y, Wang P, Liu Q, Zheng H: Current status and future perspectives of sonodynamic therapy in glioma treatment. Ultrason Sonochem 2017;37:592-599.
18 Cheng J, Sun X, Guo S, Cao W, Chen H, Jin Y, Li B, Li Q, Wang H, Wang Z, Zhou Q, Wang P, Zhang Z, Tian Y: Effects of 5-aminolevulinic acid-mediated sonodynamic therapy on macrophages. Int J Nanomedicine 2013;8:669-676.
19 Wang H, Yang Y, Chen H, Dan J, Cheng J, Guo S, Sun X, Wang W, Ai Y, Li S, Li Z, Peng L, Tian Z, Yang L, Wu J, Zhong X, Zhou Q, Wang P, Zhang Z, Cao W, Tian Y: The predominant pathway of apoptosis in thp-1

macrophage-derived foam cells induced by 5-aminolevulinic acid-mediated sonodynamic therapy is the mitochondria-caspase pathway despite the participation of endoplasmic reticulum stress. Cell Physiol Biochem 2014;33:1789-1801.

20 Li Z, Sun X, Guo S, Wang L, Wang T, Peng C, Wang W, Tian Z, Zhao R, Cao W, Tian Y: Rapid stabilisation of atherosclerotic plaque with 5-aminolevulinic acid-mediated sonodynamic therapy. Thromb Haemost 2015;114:793-803.

21 Wang Y, Wang W, Xu H, Sun Y, Sun J, Jiang Y, Yao J, Tian Y: Non-lethal sonodynamic therapy inhibits atherosclerotic plaque progression in apoe-/- mice and attenuates ox-ldl-mediated macrophage impairment by inducing heme oxygenase-1 Cell Physiol Biochem 2017;41:2432-2446.

22 Hansson GK, Robertson AK, Soderberg-Naucler C: Inflammation and atherosclerosis. Annu Rev Pathol 2006;1:297-329.

23 Galmiche A, Rassow J, Doye A, Cagnol S, Chambard JC, Contamin S, de Thillot V, Just I, Ricci V, Solcia E, Van Obberghen E, Boquet P: The n-terminal 34 kda fragment of helicobacter pylori vacuolating cytotoxin targets mitochondria and induces cytochrome c release. EMBO J 2000;19:6361-6370.

24 Ridker PM, Everett BM, Thuren T, MacFadyen JG, Chang WH, Ballantyne C, Fonseca F, Nicolau J, Koenig W, Anker SD, Kastelein JJP, Cornel JH, Pais P, Pella D, Genest J, Cifkova R, Lorenzatti A, Forster T, Kobalava Z, Vida-Simiti L, Flather M, Shimokawa H, Ogawa H, Dellborg M, Rossi PRF, Troquay RPT, Libby P, Glynn RJ: Antiinflammatory therapy with canakinumab for atherosclerotic disease. N Engl J Med 2017;377:1119-1131.

25 Ridker PM, MacFadyen JG, Everett BM, Libby P, Thuren T, Glynn RJ: Relationship of c-reactive protein reduction to cardiovascular event reduction following treatment with canakinumab: A secondary analysis from the cantos randomised controlled trial. Lancet 2017

26 Iinuma S, Farshi SS, Ortel B, Hasan T: A mechanistic study of cellular photodestruction with 5-aminolaevulinic acid-induced porphyrin. Br J Cancer 1994;70:21-28.

27 Peng Q, Moan J, Nesland JM: Correlation of subcellular and intratumoral photosensitizer localization with ultrastructural features after photodynamic therapy. Ultrastruct Pathol 1996;20:109-129.

28 Ji Z, Yang G, Vasovic V, Cunderlikova B, Suo Z, Nesland JM, Peng Q: Subcellular localization pattern of protoporphyrin ix is an important determinant for its photodynamic efficiency of human carcinoma and normal cell lines. J Photochem Photobiol B 2006;84:213-220.

29 Van Vre EA, Ait-Oufella H, Tedgui A, Mallat Z: Apoptotic cell death and efferocytosis in atherosclerosis. Arterioscler Thromb Vasc Biol 2012;32:887-893.

30 Kojima Y, Weissman IL, Leeper NJ: The role of efferocytosis in atherosclerosis. Circulation 2017;135:476-489.

31 Reth M: Hydrogen peroxide as second messenger in lymphocyte activation. Nat Immunol 2002;3:1129-1134.

32 Zhu J, Yamane H, Paul WE: Differentiation of effector cd4 t cell populations (*). Annu Rev Immunol 2010;28:445-489.

33 Kesarwani P, Murali AK, Al-Khami AA, Mehrotra S: Redox regulation of t-cell function: From molecular mechanisms to significance in human health and disease. Antioxid Redox Signal 2013;18:1497-1534.

34 Belikov AV, Schraven B, Simeoni L: T cells and reactive oxygen species. J Biomed Sci 2015;22:85.

35 Snelgrove RJ, Edwards L, Williams AE, Rae AJ, Hussell T: In the absence of reactive oxygen species, t cells default to a th1 phenotype and mediate protection against pulmonary cryptococcus neoformans infection. J Immunol 2006;177:5509-5516.

36 King MR, Ismail AS, Davis LS, Karp DR: Oxidative stress promotes polarization of human t cell differentiation toward a t helper 2 phenotype. J Immunol 2006;176:2765-2772.

37 Shatynski KE, Chen H, Kwon J, Williams MS: Decreased stat5 phosphorylation and gata-3 expression in nox2-deficient t cells: Role in t helper development. Eur J Immunol 2012;42:3202-3211.

38 Li-Weber M, Giaisi M, Treiber MK, Krammer PH: Vitamin e inhibits il-4 gene expression in peripheral blood t cells. Eur J Immunol 2002;32:2401-2408.

39 Sies H, Berndt C, Jones DP: Oxidative stress. Annu Rev Biochem 2017;86:715-748.

40 McHale AP, Callan JF, Nomikou N, Fowley C, Callan B: Sonodynamic therapy: Concept, mechanism and application to cancer treatment. Adv Exp Med Biol 2016;880:429-450.

41 Humphrey VF: Ultrasound and matter--physical interactions. Prog Biophys Mol Biol 2007;93:195-211.

42 Frostegard J, Ulfgren AK, Nyberg P, Hedin U, Swedenborg J, Andersson U, Hansson GK: Cytokine expression in advanced human atherosclerotic plaques: Dominance of pro-inflammatory (th1) and macrophage-stimulating cytokines. Atherosclerosis 1999;145:33-43.